Environmental Assessment of Land Surface Temperature Using Remote Sensing Technology

Hebah Kamal*, Munairah Aljeri, Ahmed Abdelhadi, Megha Thomas, Alyaa Dashti
System and Software Development Department, Kuwait Institute for Scientific Research, Kuwait City 24885, Kuwait

*Corresponding author: hbaron@kisr.edu.kw

The rapid growth of urbanization exposes the environment to severe issues that threaten the quality of life. High land surface temperature (LST) is one of the most prominent issues in large cities where anthropogenic activities are accumulated, energy consumption and gas emissions increase, forming urban heat islands (UHI). In this research, the LST and the UHI formations were used as indicators to inspect and evaluate the environmental status of Kuwait's urban area, which recently recorded a notable rise in air temperature. The LST spatial and temporal changes were examined and analyzed by utilizing satellite images of Landsat-8 for the period 2013–2020. The relationship between LST and air temperature was determined using the linear regression method. UHIs formation sites were investigated on different surfaces using the land use map. Results revealed that the LST average increased by 3°C in 2020 within seven years, and a strong positive relationship was observed between the LST and the air temperature. The UHI was mainly concentrated in industrial areas, oil fields, and airports. Moreover, the LST in the rural area reached 41.47°C, which is 4°C higher than it was in 2013. UHI intensity was calculated to assess the extent of variability in the LST between urban and rural areas; this intensity was lower in 2020 than in 2013 due to vegetation reduction in 2020. The continuous rise of the LST in Kuwait could lead to an inevitable environmental issue. Vegetation and water bodies play a significant role in moderating the LST, and these types of land coverage are rare in Kuwait. This research may contribute to controlling the temperature rise in UHI accumulation areas by following appropriate environmental solutions, sustainable urban planning, and encouraging the greening process.

Keywords: intensity, Landsat-8, land use, linear regression, urban heat islands.

Introduction

The world is witnessing an unprecedented speed of urbanization and population growth, confronting environmental and economic challenges around the globe. According to the World Urbanization Prospects report (2018), more than 50% of the world's population lives in urban areas today, increasingly in highly dense cities, a percentage predicted to increase to more than 68% by 2050. The United Nations Urbanization and Development report (2020) states that with the current escalation of urbanization, the gradual shift of population concentration from rural areas to urban areas, the rapid growth of population and the number of people inhabiting urban areas could increase by 2.5 billion. 96% of this increase is expected to take place in Asia and Africa.

Urbanization has positively impacted the economic growth and cultural and societal development of developing countries. Urban cities provide better access and services to health care, education, housing, social life, and security. However, rapid and unplanned urbanization can result in various numbers of global risks and challenges, including socioeconomic issues (Zhang and Li, 2020), health-related threats (Michel 2020; Lu et al., 2021), and, most importantly, the negative effect on the sustainability of the environment (Wang et al., 2014; Wang and Zhao, 2018; Hoi, 2020). Insufficient and poorly planned expansions and city development can leave urban populations vulnerable and highly exposed to the effects and impacts of climate change. Urbanization and population growth, coupled with the threat of global climate change, can cause significant risks and challenges to developing countries' physical and social environments worldwide. One of the most common consequences of the twin phenomena of urbanization and population growth is urban heat island (UHI) formation.

Oke (1982) referred to an 'urban heat island' as an urban or metropolitan region much warmer than its surrounding region. Santamouris (2015) described the UHI as local-scale heat temperature differences between urban and rural areas. A previous study has shown that heat is derived from two primary sources: solar radiation and anthropogenic heat emission (Miles and Esou, 2017). Since the physical characteristics of land cover are mainly the concentration of human development and activities, urban areas accumulate massive heat, which is the basis for forming the UHI phenomena (Lu et al., 2020). The formation and intensity of the UHI differ in space and time due to two main factors, namely meteorological factors and urban structure factors. Therefore, the UHI is significantly influenced by each city's unique characteristics, structures, and land use.

The leading cause of the UHI is the modification of the land surface by urban development. The land surface temperature (LST) varies from one place to another within the metropolitan area, and some areas reflect high temperatures. The rising temperatures of some regions are mainly caused by the thermal property of building materials, dark surfaces with low albedo and urban geometry (Solecki et al., 2005), anthropogenic heat production (Wang et al., 2018), and finally, the geographic location of the urbanized area (Ma et al., 2017). According to the United States Environmental Protection Agency (US EPA), the difference in air temperature between a city of one million inhabitants and its surroundings can be 1–3°C, and it can reach up to 12°C on a clear and calm night. Oke (1982) revealed that the UHI effect could increase the air temperature in an urban area by 2–8°C. Furthermore, several studies have shown that a strong UHI effect can increase energy consumption (Li et al., 2019), carbon emission (Rossi et al., 2016), heat waves (Tan et al., 2010), and can threaten human health (Heaviside et al., 2017).

The effects of global warming are primarily concentrated in cities due to the UHI impacts and the unique socioeconomic character of the urban environments. Existing research documents the consequences and results of extreme heat events on human health, physical infrastructure, and urban dwellers' general well-being. Landsberg (1981) stated that UHI is the most noticeable climate indicator of urbanization, and it exists in every city around the world. With an expected 4°C increase in the average annual global temperature in the coming years (Turco et al., 2018) and the current rapid increase in urbanization

worldwide, especially in developing countries, it becomes increasingly essential to understand the factors leading to the UHI phenomenon. Investigating the spatiotemporal distribution of UHIs and its effect is critical in understanding the processes of urban environmental changes and is crucial to human health.

One of the vital purposes of various UHI studies includes establishing UHI distribution and its maximum and average intensity on specific days. The intensity of the UHI has commonly been defined as the temperature difference stated at a given time between the hottest area of the city or town and the non-urban (rural) area surrounding it. According to Memon et al. (2009), the intensity of the UHI is the simplest and most quantitative indicator of the thermal changes forced by the city's land use/land cover (LULC) on the region in which the UHI is identified and of its relative warming to the neighboring rural environment.

A growing body of literature has revealed that LULC is directly associated with LST and is a significant indicator and a factor of UHI formation (Ali et al., 2016; Liu et al., 2016; Wang et al., 2016; Tran et al., 2017). Urbanization removes natural vegetation and replaces the same with buildup materials, such as concrete masses, asphalt roads, and metal surfaces and roofs. These materials are high heat absorbing, low solar reflective, water-resistant, and non-vaporization structures. The change and modification of the natural land cover due to urbanization alter the urban landscape's thermal properties. The urban land surface typically has a comparatively higher thermal capacity than non-urban areas, increasing the urban LST. Research interest in LST and UHIs has been continued by the growing and upward economic, social, environmental, and health consequences of the UHI phenomenon.

Ali et al. (2016) have conducted a valuable study on UHI distribution by sampling air temperature values at different point locations using air samplers and thermometers and interpolating the obtained temperature data point to generate a temperature surface given area of interest. Current research has focused on space-borne remote sensing imagery, broadly being used in understanding the thermal, biophysical properties and the general environmental conditions of the earth's surface (Wang et al., 2016). When studying UHIs using a remote sensing approach, LST is the entry point and the primary key parameter. LST is closely related to UHI and can offer the needed insight into the general UHI conditions. For a decade, research on the UHI effect and impact using remote sensing has been conducted at multiple spatial and temporal scales using different satellites and sensors. Such sensors can provide LST values with a high spatial resolution of 5 cm to 120 m (Estoque et al., 2017; Sattari et al., 2018). However, these sensors are mainly limited for time-series analysis when considering their long revisiting rounds and the high possibility of cloud coverage.

From the previous perspective, this research used LST and UHI as indicators to inspect and evaluate the environmental status of the urban area in the State of Kuwait in the recent period. The research objectives are initially focused on investigating and examining the spatial and temporal changes of the LST from 2013 to 2020 using medium-resolution imageries of Landsat-8. Secondly, it emphasizes determining the relationship of the LST with measured air-temperature station data and then utilizing time-series remotely sensed imagery to identify and detect the spatial distribution of the UHI in various land use. Finally, the research aims to assess the extent of LST variability between urban and rural areas through UHI intensity calculation.

Despite the importance and progressive increase of the UHI phenomenon globally and the continuous rise in Kuwait's local temperatures since the seventies (Bannari et al., 2020), limited studies have been conducted in Kuwait to understand the behavior of LSTs and the factors contributing to UHI development. The details of the only four published studies that attempted to explore and analyze the UHI in Kuwait are provided subsequently. Nasrallah et al. (1990) did descriptive statistical analyses in Kuwait on 23 years of annual air temperature data for urban and rural weather stations. They concluded that heat islands in Kuwait City were poorly identified with a low rate of temperature changes, in contrast to a study in Phoenix, Arizona, which shares a similar climate. The authors explained this difference in the city landscape and its proximity to the large water body in Kuwait.

Kwarteng and Small (2005) compared the environmental conditions between New York City (NYC) and Kuwait City to demonstrate the difference in surface temperature and vegetation abundance by analyzing Landsat-7 imagery of 2001. The analysis of the thermal behavior of Kuwait City showed that due to the cooling effects of vegetation, urban areas were colder than the surrounding desert areas, particularly in the residential areas. On the other hand, the surface temperature observed in the residential areas in NYC was higher, even though NYC has a slightly more vegetation fraction.

Uddin et al. (2010) sought to discover the relationship of LST with each of the four biophysical parameters, namely normalized difference vegetation index (NDVI), normalized difference water index (NDWI), normalized difference buildup index (NDBI), and normalized difference bareness index (NDBaI), and the correlation effect for different land cover classifications. The parameters were computed using satellite datasets for the period 1989–2000. The results showed a positive correlation of NDBI with the surface temperature and a negative correlation with the rest of the parameters.

Alahmad et al. (2020) studied LST distribution to identify the UHI and urban cool islands (UCI) formation during the four seasons in the daytime and nighttime using the MODIS satellite from 2001 to 2017. In the study, the governorates of Kuwait are divided into urban and rural areas. The governorates containing the farms were considered rural areas. The results revealed that despite some UHI zones within the metropolitan region, the urban areas appeared as cool islands during the daytime due to sea breezes that cool the coastal urban area and reduce the LST, especially in summer. The authors recommended using a high spatial resolution satellite to clarify more details and using land use data to explain the nature of land cover that raises the LST and forms hot or cold spots within the urban area.

Compared with the approaches mentioned above, the main highlights of the presented work can be listed as follows: firstly, the proposed research was focused on identifying and detecting the spatial distribution of the LST during the recent years 2013–2020 using Landsat-8 data. The role of LST as a primary factor in the high rise of air temperature was investigated by correlating and identifying the relationship between the two variables. Furthermore, it explored and evaluated the impact and influence of different land uses on UHI distribution using a detailed and updated LULC map and examined and analyzed the long-term changes in the UHI intensity pattern between the urban and rural areas. Finally, some solutions and strategies were proposed for LST reduction and UHI mitigation.

Methods

Study area

The State of Kuwait is located in the northeast corner of the Arabian Peninsula between longitudes 46.5°E and 48.5°E and latitudes 28.5°N and 30.0°N and is bordered by Iraq in the north and Saudi Arabia in the west and south. Kuwait is one of the smallest countries globally regarding land area, only around 18,000 km². According to the 2020 statistics of the Kuwait Central Administration, the total population of Kuwait is 4,464,521. Kuwait lands are characterized by flatlands that gradually rise until 360 m in Metla's area in the Arabian Gulf. Kuwait's climate is characterized by two main seasons: a long hot and dry summer and a short and low precipitation winter that extends for approximately three months, from December to February. The urban area is located in the southern part of Kuwait Bay, extending to the southern borders along the coast. The study area (*Fig. 1*) is determined to include the various land uses in the country. Land use in the urban area varies between residential, commercial, industrial, and small agricultural areas in Sulaybiya, Al-Wafra, and the western desert areas.

Dataset

Satellite Data

The Landsat-8 OLI and TIRS satellite data from 2013 to June 2020 were downloaded from the USGS website. Landsat-8 band specifications are represented in *Table 1* (Reddy and Manikiam, 2017). The subset tool was used to clip the image to the specified study area, as this is considered a vital pre-step before applying any function or analysis.

Fig. 1. *Location map of the study area (source: created using ArcMap software)*
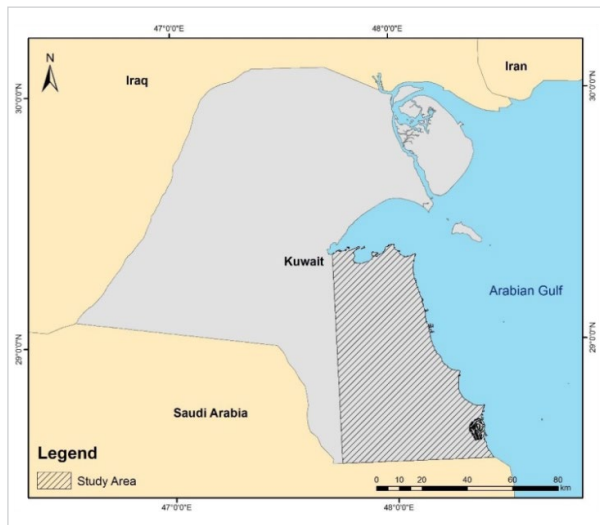
Table 1. *Landsat-8 OLI and TIRS Bands Specifications*

Bands	Wavelength (micrometers)	Resolution (meters)
Band 1 – Coastal aerosol	0.43–0.45	30
Band 2 – Blue	0.45–0.51	30
Band 3 – Green	0.53–0.59	30
Band 4 – Red	0.64–0.67	30
Band 5 – Near Infrared (NIR)	0.85–0.88	30
Band 6 – SWIR 1	1.57–1.65	30
Band 7 – SWIR 2	2.11–2.29	30
Band 8 – Panchromatic	0.50–0.68	15
Band 9 – Cirrus	1.36–1.38	30
Band 10 – Thermal Infrared (TIRS) 1	10.6–11.19	100
Band 11 – Thermal Infrared (TIRS) 2	11.50–12.51	100

Source: Reddy and Manikiam, 2017.

Meteorological Data

The air temperature data were collected from the General Administration of Civil Aviation/Meteorological Department, Kuwait, for the exact dates of the satellite data. The retrieved data observation included the maximum, minimum, and average air temperature measurements. *Fig. 2* shows the distribution of seven weather stations in the study area.

Fig. 2. *Meteorological stations in the study area (source: created using ArcMap software)*


Land Use Data

The land use map for 2018 was obtained from Kuwait Institute for Scientific Research (KISR). *Fig. 3* shows the distribution of different land uses in the study area based on the received data. The purpose was to reveal the land use type with higher UHI distribution.

Methodology

Fig. 4. summarizes the methods followed for UHI map production in the study area. The 'RSandGIS V17.0' plugin (Prathamesh) is available in open-source Quantum GIS (QGIS) software used to calculate LST. The equations used in the plugin for generating the LST are explained in the upcoming sections.

2018 Land use map of the study area (source: created using ArcMap software)
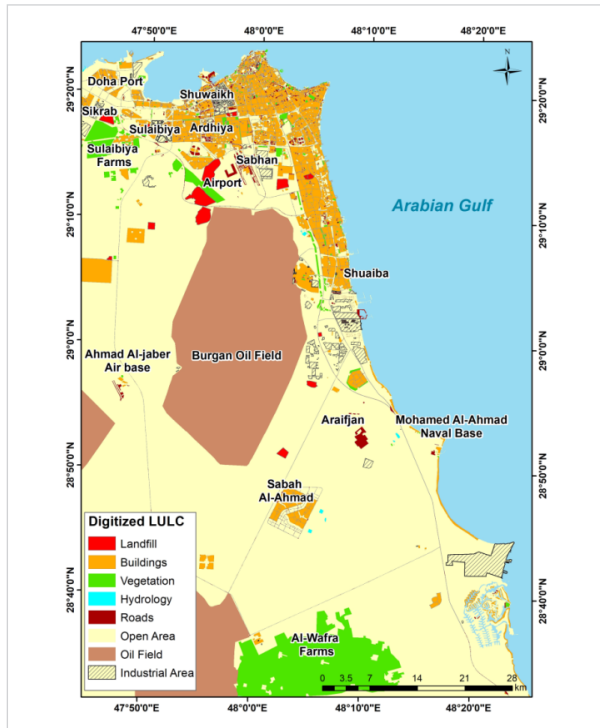
Fig. 4. *Flow chart of UHI map production (source: created using Microsoft Visio software)*
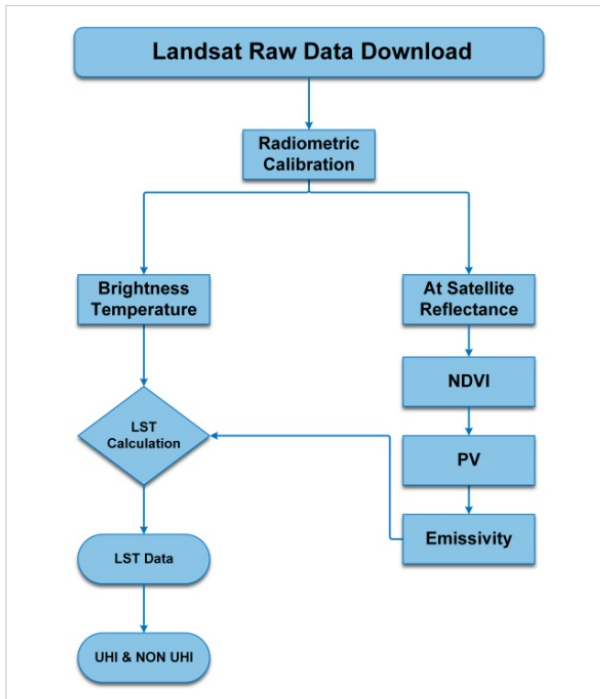
Satellite Data Preprocessing

The acquired satellite data were subjected to distortion due to sensor, solar, and atmospheric effects and required image preprocessing before any analysis to minimize distortion. The images were subjected to atmospheric correction methods, which included the subsequent two processes as follows:

– Radiometric calibration. The calibration converts the image's digital numbers (DN) to radiance. Radiance is the parameter measured at the sensor. It is dependent on surface reflectance in the given direction, but reflectance is the solar radiation reflected from different objects on the earth's surface. Initially, the images are converted to radiance through radiometric calibration. The radiometric calibration is applied to all satellite images using equation 1.

$$L_\lambda = M_L * Q_{cal} + A_L \qquad (1)$$

Where: Q_{cal} is the quantized and calibrated standard product pixel values (DN);

M_L is the band-specific multiplicative rescaling factor from Landsat metadata;

A_L is the band-specific additive rescaling factor from Landsat metadata.

– Top of the atmosphere reflectance. After altering the image to radiance, the output must be converted to top of atmosphere (TOA) reflectance to measure the actual solar radiation reflected from each surface on the earth after removing the atmospheric effects. Equation 2 is applied to reverse the radiance to reflectance.

$$R_\lambda = M_R * Q_{cal} + A_R \qquad (2)$$

Where: Q_{cal} is the quantized calibrated pixel value in DN;

M_R is the band-specific reflectance multiplicative scaling factor;

A_R is the band-specific reflectance additive scaling factor.

Land Surface Temperature Retrieval

– Brightness temperature calculation. Brightness temperature (BT), NDVI, and vegetation proportion (P_V) are needed to calculate emissivity(ε) and LST.

A satellite BT algorithm is used to convert thermal (TIR) bands (bands 10 and 11) to reflectance using equation 3.

$$BT = \frac{K2}{\ln(\frac{K1}{L_\lambda} + 1)} - 273.15 \tag{3}$$

Where: $K1$ and $K2$ are the band-specific thermal conversion constant from the satellite image metadata.

– Normalized difference vegetation index calculation. NDVI was calculated to obtain the land surface emissivity, and it is defined as the average emissivity of an element on the earth's surface calculated from the measured radiance and LST. To calculate emissivity for different land use in the study area, NDVI was calculated using equation 4.

$$NDVI = (NIR - RED)/(NIR + RED) \tag{4}$$

– Vegetation proportion calculation. P_v is the main input for obtaining emissivity, and it is the proportion of the perpendicular projection region of the plants on the land to the total green area, as indicated in equation 5.

$$P_v = (\frac{NDVI - NDVI_{min}}{NDVI_{max} - NDVI_{min}})^2 \tag{5}$$

– Emissivity calculation. Emissivity (ε) is the relative ability of the material's surface to emit energy by radiation and is calculated using equation 6.

$$\varepsilon = 0.004 * P_v + 0.986 \tag{6}$$

Where: 0.004 is the constant value taken for surface roughness, and 0.986 is the average image emissivity.

– LST calculation. The outputs of the past equations are used as inputs for the LST, calculated based on equation 7.

$$LST = \frac{BT}{1 + [\left(\frac{\lambda BT}{\rho}\right) \ln \varepsilon]} \tag{7}$$

Where: λ is the average wavelength of TIR bands in μm;
$\rho = h*c/\sigma$ (1.438 x 10–2mK);
σ = Boltzmann constant (1.38 x 10–23 J/K);
h = Plank's constant (6.626 x 10–34Js);
c = velocity of light (3 x 108 m/s).

Relationship Identification between LST and Air Temperature

Data for summer 2013–2020 were located on Kuwait's map based on the seven stations' geographic locations using the Arc Map software. Correlation analysis using linear regression (Weisberg, 2005) was carried out to identify and analyze the relationship between the two variables.

Urban Heat Island Detection and Classification

– UHI derivation. Guha et al. (2020) have provided details of the equation to be applied to each LST map (Equation 8) to identify UHI and non-UHI areas in different years.

$$LST > μ + 0.5 * δ$$
$$0 < LST < μ + 0.5 * δ \tag{8}$$

Where: μ is the mean LST and δ is the LST standard deviation.

– UHI intensity. El-Hattab et al. (2018) have defined intensity as the difference in the LST between urban and rural areas. The LST is lower in cultivated areas due to the role of vegetation in cooling and reducing temperatures, unlike other urbanized areas (Wang et al., 2018). To assess the extent of variability in surface temperatures between urban areas and vegetation cover in 2013 and 2020, urban and rural areas were identified by drawing two separate polygons. The first polygon included urban and anthropogenic land uses like buildup areas, industrial areas, airports, roads, and Burgan field. The second polygon was drawn around Sulaibiya farms, chosen as the rural area due to vegetation density and the regular cultivation pattern.

Results and Discussion

Land surface temperature analysis

LST maps illustrated in *Fig. 5* show a notable temperature rise in specific areas. Temperature classification is standardized in all maps ranging from 19 to 65°C. The water bodies recorded the lowest temperature at 19°C. In contrast, the highest temperature of 65°C in the fiery flame in Shuaiba industrial port and Burgan oil field appeared as hot spots on LST maps. The land use map for 2018 was used to analyze the LST in the study area.

The map (*Fig. 5a*) illustrates a general LST decrease in 2013 with an average of 42.3°C (*Fig. 6*). The area witnessed lower temperatures than in the following years (*Figs. 5b–5h*). The LST average increased gradually to reach the peak of 50°C in 2017 (*Fig. 6*), where the temperatures in most study areas ranged between 47°C and 54°C (*Fig. 5e*). After 2017, the LST started fluctuating until it reached 45.2°C in 2020 (*Fig. 6*), reflecting a difference of 3°C within only seven years compared with 2013.

From the aforementioned, the LST maps had irregular patterns throughout the periods under study. The same fluctuations were observed before by Uddin et al. (2010) with a continuous rise in the LST average. However, the climatic characteristics of the arid regions can be a significant factor leading to this irregularity, such as local winds, solar loads (Nasrallah et al., 1990), oceanic circulation, and annual precipitation rates contributing to increasing vegetation cover and soil moisture.

Despite the variation in the LST through the investigated years, there were significant features prevalent in the study area. It was observed through visual interpretation that the residential and commercial spaces located close to the coast recorded a lower LST, especially in Ras Al-Salmiya and Kuwait City (the capital), than in the inland regions. Alahmad et al. (2020) have mentioned that coastal areas are exposed to the sea breeze, which cools and lowers the temperature. Some regions, represented by oil fields, industrial sites, the airports, and even marine ports, recorded the highest LST at 44–51°C. Furthermore, Al-Sulaibiya farms and Al-Khairan lakes were in the lowest LST ranges, 19–35°C on all dates, due to the nature of their land cover.

Correlation analysis between LST and air temperature

Since the 1970s, meteorological stations in Kuwait have recorded an increase in average temperature by 2.2°C (Bannari et al., 2020). Therefore, the relationship between air temperature and the produced LST was examined to determine the impact of surface temperatures on local weather. *Figs. 7a* and *7b* illustrate the result of applying simple linear regression to the LST and air temperature for the selected years. The linear regression result showed that the variables between 2013 and 2020 had a correlation coefficient of $R^2 = 0.66$, indicating a strong positive relationship between the LST and the air temperature, demonstrating the role of the LST as one of the main factors leading to the rising air temperature in the area. It is an alarming indicator, especially with the high recorded LST, which could lead to more air temperature rising in the future.

Spatio-temporal analysis of urban heat island

Spatial distribution of UHI

After examining and analyzing the LST maps, equation (8) was applied to identify UHI and non-UHI areas in different years to determine the land uses that contributed to the UHI formation in the study area. The spatial distribution of UHI for 2013–2020 is illustrated in *Fig. 8*. The total study area is about 4435 km²; UHIs occupy between 1200–1400 km², which is approximately 30% of the study area in all the studied years (*Fig. 9*). The 2018 land use map was used to identify land uses contributing to the UHI formation. The UHI was formed in the highest LST in certain land use:

_ Oil fields, such as Burgan, Umm Gudair, Khashman, and AlWafraa. In all the investigated years, the oil fields formed UHI, and especially the Burgan oil field, which spread at 562 km², showed a huge heat island in the middle of the study area, except for some artificial water lakes within the field border, which appeared as non-UHI areas.

Fig. 5. *Land surface temperature maps for the selected years: (a) 2013, (b) 2014, (c) 2015, (d) 2016, (e) 2017, (f) 2018, (g) 2019, (h) 2020 (source: LST generated using 'RSandGIS V17.0' plugin in QGIS software and temperature classification done in ArcMap software)*
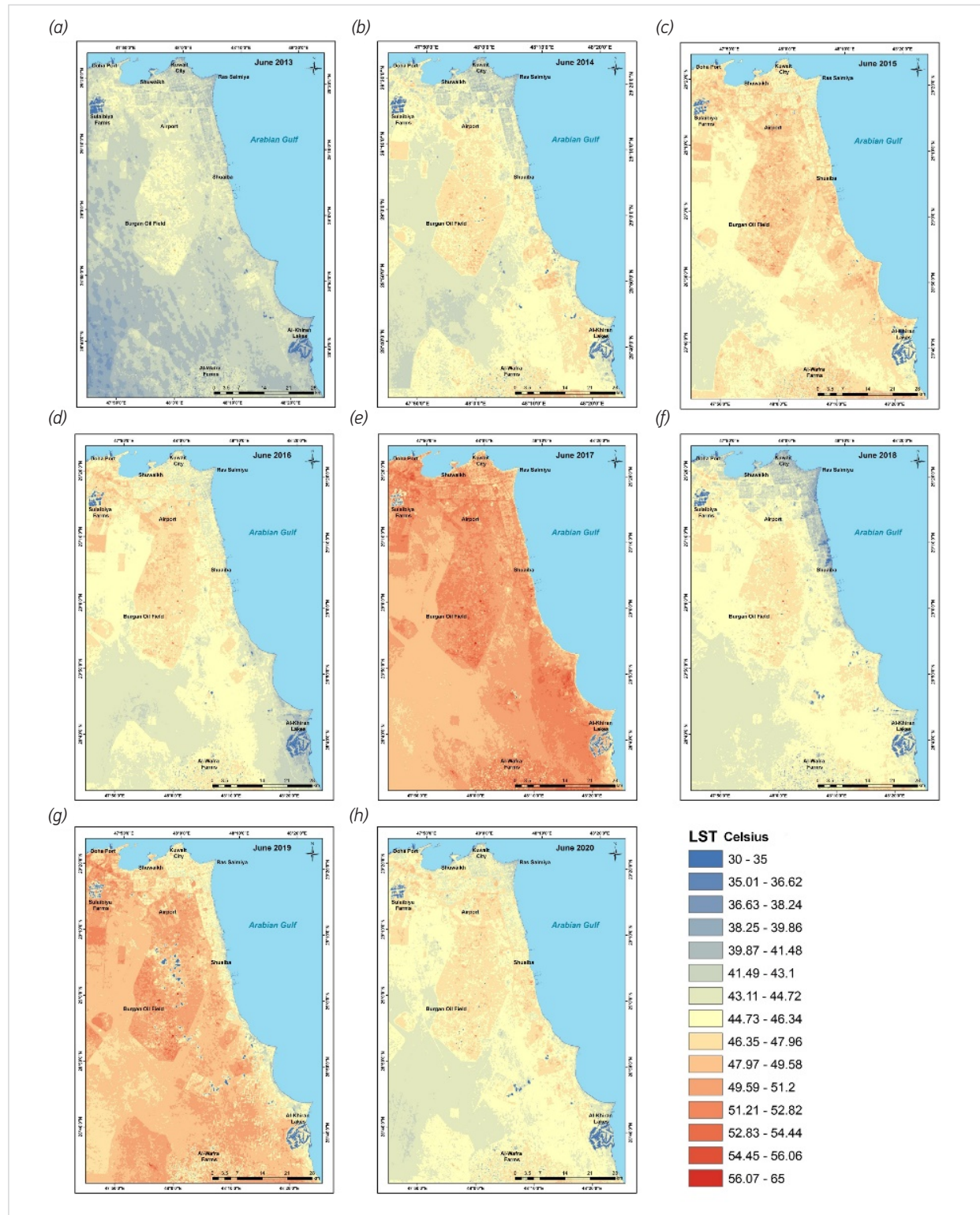
Fig. 6. *Mean land surface temperature for the years 2013–2020 (source: created using Microsoft Excel software)*
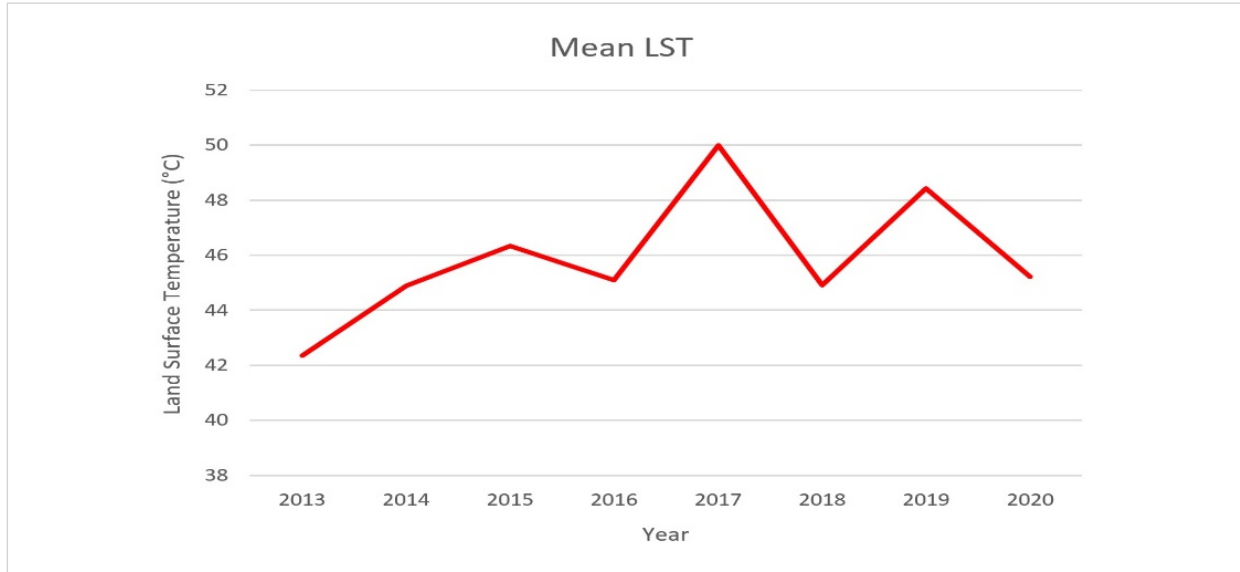

Fig. 7. *Land surface temperature and air temperature correlation analysis: (a) relationship between LST and air temperature, (b) yearly correlation between LST and air temperature (source: created using Microsoft Excel software)*
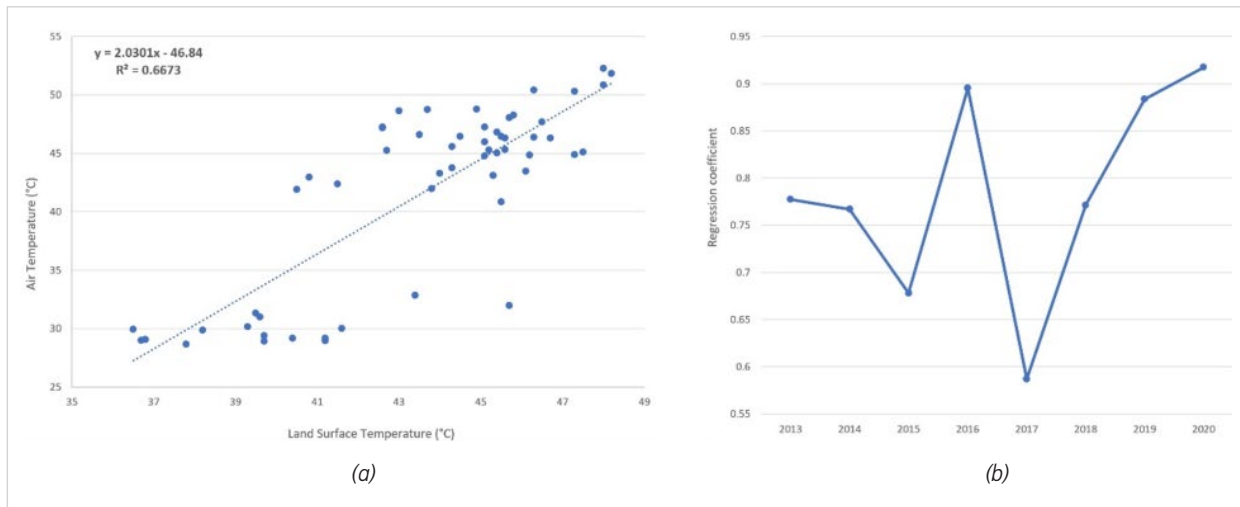

_ Industrial areas and ports. The industrial areas in Shuwaikh, Doha Port, Shuaiba port, Sabhan, Ahmadi, Sicrab area, Ardhiya, and Doha south station were marked as heat islands, and they were more concentrated in most of the years (*Figs. 8a, 8c, 8d, 8e, 8h*).

_ Kuwait Airport area, airbases, and army camps. Kuwait airport, located in the east of the Sabhan industrial area and south of Dhajeej commercial site that includes many commercial activities and government departments, is one of the most prominent UHI areas. Despite the airport closure in June 2020 due to the Covid-19 pandemic (Velavan and Meyer, 2020), the area was still marked as UHI. In addition to the main airport, the UHI was formed in the Ahmad al-Jaber air base, Mohammad al-Ahmad Kuwaiti naval base, the army bases at Camp Arifjan, and the military bases (*Figs. 8a, 8h*).

Fig. 8. *Urban heat island maps for the selected studied years: (a) 2013, (b) 2014, (c) 2015, (d) 2016, (e) 2017, (f) 2018, (g) 2019, (h) 2020 (source: created using ArcMap software)*
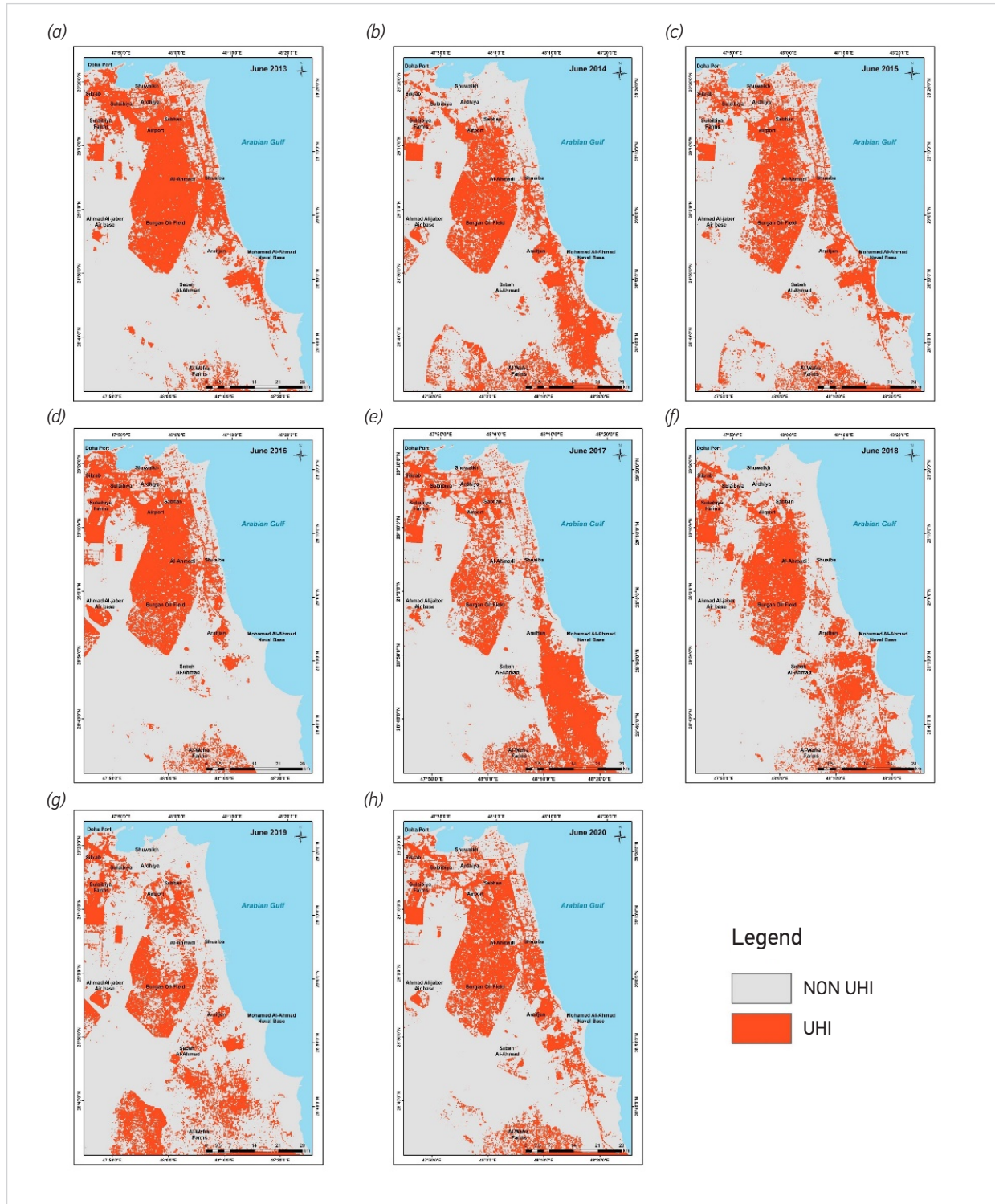
Fig. 9. *Area of urban heat islands in each studied year (source: created using Microsoft Excel software)*
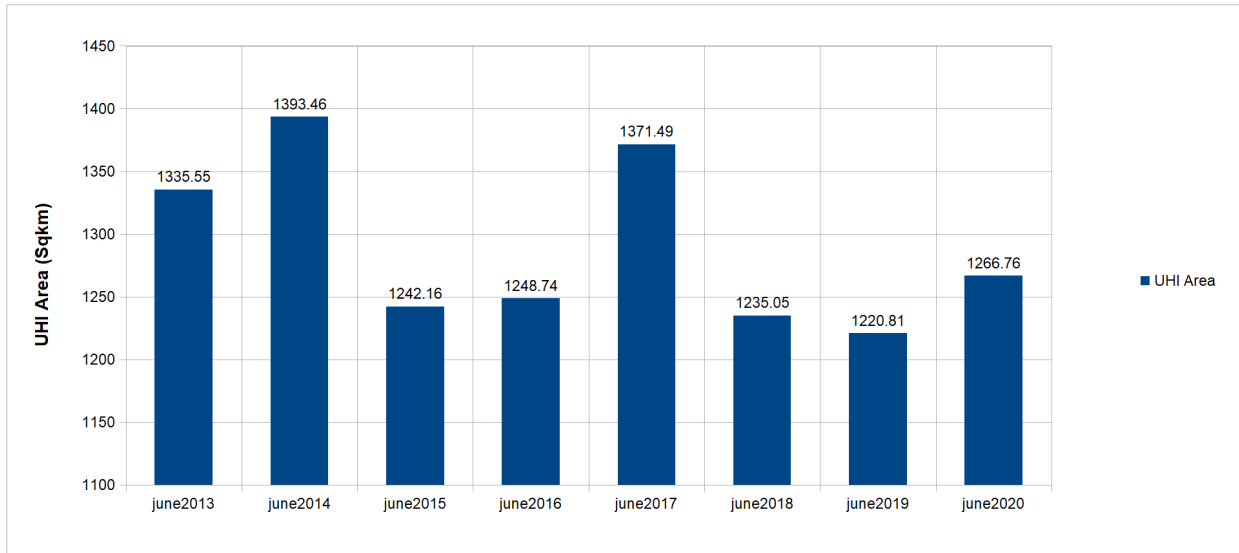

Trapped empty spaces, asphalt surfaces, and landfills. The open spaces between the build-up appeared as UHI (*Fig. 10*), for example, the Al-Siddiq residential area (*Fig. 10d*), specific blocks in Bayan (*Fig. 10e*), unconstructed areas of the medical campus of Kuwait University in Al-Shadadiya (*Fig. 10c*), open space next to Bayan Palace and Doha port area, and the cemetery areas (*Fig. 10b*). Likewise, UHIs are formed on asphalt surfaces, whether in urban areas, such as the Sabah Al-Ahmad Square shooting complex (*Fig. 10a*) or in the desert, such as the Camel Club racetrack (*Fig. 10f*). Moreover, some landfills and their surrounding regions have formed a very dense UHI between residential areas or outskirts facing the desert, as shown in the land use map (*Fig. 3*).

Alahmad et al. (2020) have reported that the coarse resolution of MODIS did not support identifying hot or cool islands within the urban area. Therefore, they considered the coastal area an urban cool island (UCI) during the daytime. Whereas Landsat-8 has proven its effectiveness in locating and monitoring UHIs, especially in the residential and commercial regions extended along the coastal zone, these areas have retained their low temperatures during the day, but an UHI still forms through their lands. Although the UHI phenomenon is most intense during the night, it still

occurs in the daytime all year round (Leal Filho et al., 2017), as it frequently appears in the open yards and large asphalt car parking along the coastal area. The UHI's existence in such locations is a consequence of the air trapping between dense buildings constructed of high thermal absorbing materials and the narrow asphalt roads, hindering heat exit from this area and thus the physical cooling process (Rasul, 2016).

On the other hand, the UCIs were formed in the big parks and gardens within the urban area, such as in Al Shaheed Park in Kuwait City. Vegetation works on decreasing the near-surface air temperatures by an average of 1–4.7°C (Kleerekoper et al., 2012). In this regard, Kwarteng and Small (2005) studied the role of vegetation in cooling urban areas and lowering the LST, emphasizing to city planners in Kuwait to pay attention to industrial areas where artificial activities occur with little or no vegetation cover. Unfortunately, the recent satellite images showed that scattered, unplanned desert plants still intersperse these areas. The vegetation scarcity, besides emitted gases, pollutants, and the nature of the buildings' construction materials, specially curved sheet metal and asphalt surfaces, which spread in the industrial areas, all contributed to the LST continuous rising and, therefore, the UHI formation.

Fig. 10. *High-resolution satellite image displaying UHI formation in trapped empty spaces and asphalt surfaces (source: created using ArcMap software)*
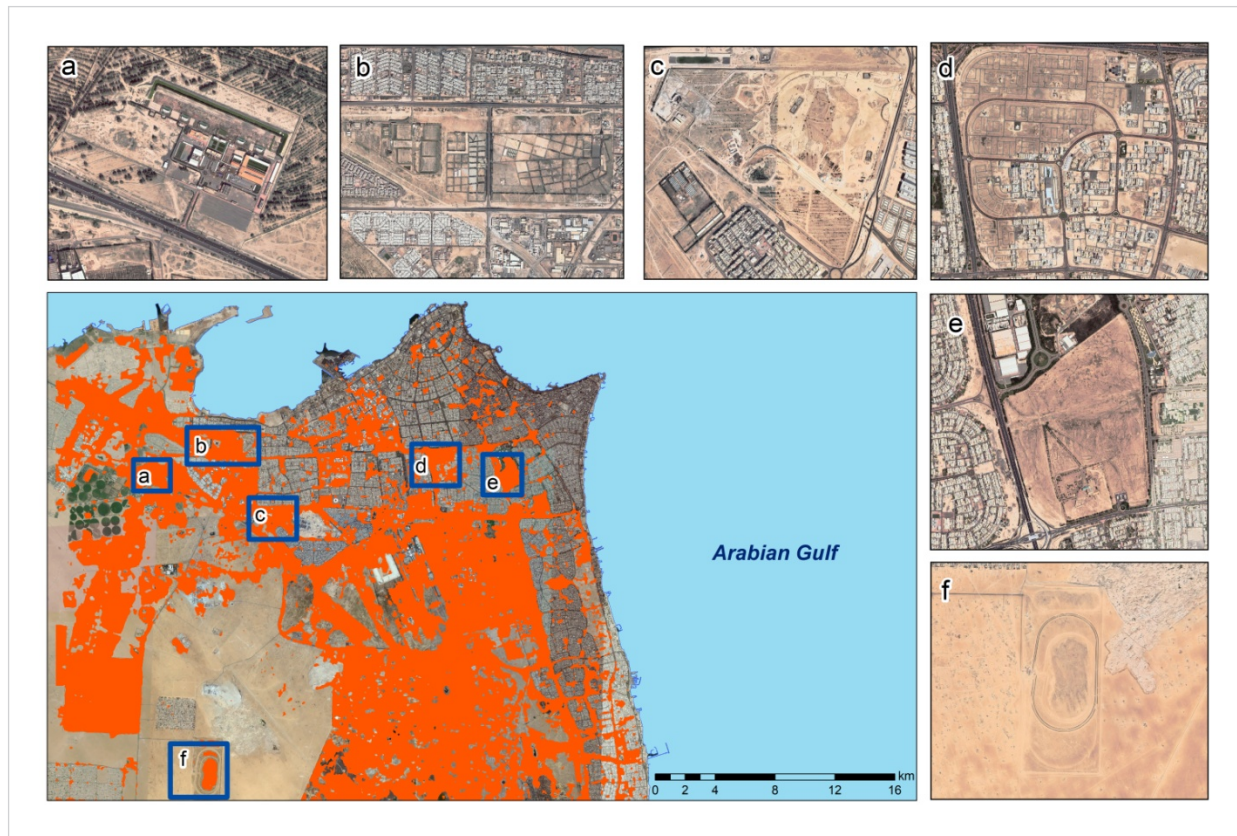
Overall, the high LST and UHI formations were related to specific land uses pertinent to anthropogenic activities in Kuwait, confirming the role of urbanization in generating UHIs. Experts have confirmed that the increase in population could increase the impact of cities on the regional climate in particular and the global climate in general (Leal Filho et al., 2017). The latest population statistics published by the Public Authority for Civil Information official website state that Kuwait's population has increased by more than 700,000 people during the past seven years. Unquestionably, this steady increase in the population means more waste heat from traffic and an increase in energy demand for cooling by air conditioners, especially in summer (Leal Filho et al., 2017), which leads to more greenhouse gasses emissions and heatwaves, thus, generating a higher LST.

Temporal intensity of UHIs

UHI intensity results indicated the continuous increase of the LST in urban and rural areas over Kuwait. *Table 2* shows the mean LST and UHI intensity in the urban and rural regions of the study area in 2013 and 2020. The LST increased in 2020 by 4°C in rural areas and 2.61°C in urban areas compared with 2013. The UHI intensity was 5.62 in 2013, and the intensity was 4.22 in 2020 due to rural area's LST rising.

The NDVI for 2013 and 2020 were calculated to identify the reasons for increased LST in Sulaibiya farms in 2020 (*Table 3*). Results showed that the percentage of highly dense vegetation cover on the farms in 2020 was lower than in 2013, explaining the recent LST rise in the farms and low intensity, emphasizing the role of vegetation in moderating surface temperature.

Table 2. *Variations of UHI intensity in 2013 and 2020*

Year	LST (Urban area)	LST (rural area)	Intensity
2013	43.08	37.46	5.62
2020	45.69	41.47	4.22

Source: mean LST and intensity were calculated using ArcMap software.

Table 3. *Calculation of NDVI parameter for Sulaibiya farms in 2013 and 2020.*

NDVI Range	NDVI Type	Area (%) – 2013	Area (%) – 2020
NDVI > 0.4	High vegetation	44.12	36.54
0.2 < NDVI < 0.4	Low vegetation	34.15	40.61
NDVI < 0.2	Non vegetation	21.10	22.14

Source: NDVI was calculated using ArcMap software.

Proposed strategies for LST reduction and UHI mitigation

According to the Arab National Development Planning Portal, Kuwait's national development plan, "New Kuwait 2035", comprises seven main pillars that align with the UN's sustainable development goals (SDG). "Sustainable living environment" is one of the seven pillars based on the group of SDG goals, including climate action, life on earth, and sustainable cities and communities. Therefore, climatic changes and global warming are considered the challenges obstructing the country's development. LST variations and UHIs formations located in the produced maps will assist in guiding the suitable solution for LST reduction and UHI mitigation in each area.

For example, in the capital of the country "Kuwait City" (the commercial and finance center), with high dense buildings and towers, applying the greening mechanism by planting shade trees and utilizing green roofs (Nuruzzaman, 2015) could contribute to LST reduction and cooling the atmosphere. Furthermore, promoting the implementation of parks and artificial lakes within open areas in the urban area will directly prevent UHIs from forming.

The sustainable urban infrastructure mechanism could also be applied (Leal Filho et al., 2017) to industrial areas' buildings. The sustainable infrastructure concept works on reducing the building's absorption of solar heat by applying light-colored roofs and high Albedo materials (Nuruzzaman, 2015), reducing the energy consumed in cooling the building. In addition, utilizing high albedo pavement on open asphalt surfaces will prevent UHI formation.

Air conditioners are used 24 hours a day in all types of urban facilities and buildings because of the high temperature in Kuwait, especially in summer. Leal Filho et al. (2017) mentioned the harmful role of traditional cooling systems in adding heat to the atmosphere; the geothermal energy and radiation-cooling systems could be a powerful alternative to air conditioners in Kuwait.

Conclusion

This study focused on utilizing remote sensing tools and technologies to observe and evaluate the environmental impacts of urbanization on the LST and the UHI formation in the State of Kuwait for the period 2013–2020. The medium resolution of Landsat-8 data assisted in monitoring LST variation in different land uses, therefore, locating UHI within the urban areas during the daytime. The period under study witnessed a continuous increase in the LST, reaching 45.2°C in 2020 with a difference of 3°C compared with 2013. Specific land uses caused the UHI formation in Kuwait, but the oil fields and industrial areas were considered primary contributors. The green spaces and lakes recorded the lowest LST and appeared as UCIs, yet such surfaces have a limited spread in the Kuwait urban area. Moreover, the resultant strong positive relation between the LST and the air temperature confirmed the direct effect of the high surface temperature on the rising air temperature.

Furthermore, the LST average in both urban and rural areas increased in 2020, where the decrease in vegetation density of Sulibiya farms led to a higher LST average of 4°C compared with 2013; hence more concern and efforts are needed in the agricultural

aspect. Specialists in environmental management and decision-makers in Kuwait can benefit from the produced maps and the suggested solution strategies in the context of achieving the "sustainable living environment" pillar included in Kuwait's national development plan 2035. LST can be tracked in the future using the previous methodology.

References

Alahmad, B., Tomasso, L.P., Al-Hemoud, A., James, P. and Koutrakis, P., 2020. Spatial distribution of land surface temperatures in Kuwait: Urban Heat and Cool Islands. International journal of environmental research and public health, 17(9), p.2993. https://doi.org/10.3390/ijerph17092993

Ali, J.M., Marsh, S.H. and Smith, M.J., 2016. Modelling the spatiotemporal change of canopy urban heat islands. Building and Environment, 107, pp.64-78. https://doi.org/10.1016/j.buildenv.2016.07.010

Bannari, A., and Al-Ali, Z. M., 2020.Assessing climate change impact on soil salinity dynamics between 1987-2017 in arid landscape using Landsat TM, ETM+ and OLI data. Remote Sensing, 12(17), 2794. https://doi.org/10.3390/rs12172794

El-Hattab, M., Amany, S.M. and Lamia, G.E., 2018. Monitoring and assessment of urban heat islands over the Southern region of Cairo Governorate, Egypt. The Egyptian Journal of Remote Sensing and Space Science, 21(3), pp.311-323. https://doi.org/10.1016/j.ejrs.2017.08.008

Estoque, R.C., Murayama, Y. and Myint, S.W., 2017. Effects of landscape composition and pattern on land surface temperature: An urban heat island study in the megacities of Southeast Asia. Science of the Total Environment, 577, pp.349-359. https://doi.org/10.1016/j.scitotenv.2016.10.195

Guha, S., Govil, H., Dey, A. and Gill, N., 2020. A case study on the relationship between land surface temperature and land surface indices in Raipur City, India. GeografiskTidsskrift-Danish Journal of Geography, 120(1), pp.35-50. https://doi.org/10.1080/00167223.2020.1752272

Heaviside, C., Macintyre, H. and Vardoulakis, S., 2017. The urban heat island: implications for health in a changing environment. Current environmental health reports, 4(3), pp.296-305.https://doi.org/10.1007/s40572-017-0150-3

Hoi, H.T., 2020, July. Impacts of Urbanization on the Environment of Ho Chi Minh City. In IOP Conference Series: Earth and Environmental Science (Vol. 505, No. 1, p. 012035). IOP Publishing. https://doi.org/10.1088/1755-1315/505/1/012035

Kleerekoper, L., Van Esch, M., and Salcedo, T. B. (2012). How to make a city climate-proof, addressing the urban heat island effect. Resources, Conservation and Recycling, 64, 30-38.https://doi.org/10.1016/j.resconrec.2011.06.004

Kwarteng, A.Y. and Small, C., 2005. Comparative analysis of thermal environments in New York City and Kuwait City. In Proceedings of the Remote Sensing of Urban Areas, Tempe, AZ, USA, 14-16 March 2005; pp. 14-16.

Landsberg, H.E., 1981. The urban climate. Academic press.

Leal Filho, W., Echevarrialcaza, L., Emanche, V. O., andQuasem Al-Amin, A. (2017). An evidence-based review of impacts, strategies and tools to mitigate urban heat islands. International journal of environmental research and public health, 14(12), 1600. https://doi.org/10.3390/ijerph14121600

Li, X., Zhou, Y., Yu, S., Jia, G., Li, H. and Li, W., 2019. Urban heat island impacts on building energy consumption: A review of approaches and findings. Energy, 174, pp.407-419. https://doi.org/10.1016/j.energy.2019.02.183

Liu, K., Su, H., Li, X., Wang, W., Yang, L. and Liang, H., 2016. Quantifying spatial-temporal pattern of urban heat island in Beijing: An improved assessment using land surface temperature (LST) time series observations from LANDSAT, MODIS, and Chinese new satellite GaoFen-1. IEEE Journal of Selected Topics in Applied Earth Observations and Remote Sensing, 9(5), pp.2028-2042. https://doi.org/10.1109/JSTARS.2015.2513598

Lu, D., Xu, J., Yue, W., Mao, W., Yang, D. and Wang, J., 2020. Response of PM2. 5 pollutions to land use in China. Journal of Cleaner Production, 244, p.118741. https://doi.org/10.1016/j.jclepro.2019.118741

Lu, X., Yuan, D., Chen, Y. and Fung, J.C., 2021. Impacts of urbanization and long-term meteorological variations on global PM2. 5 and its associated health burden. Environmental Pollution, 270, p.116003. https://doi.org/10.1016/j.envpol.2020.116003

Ma, S., Pitman, A., Hart, M., Evans, J.P., Haghdadi, N. and MacGill, I., 2017. The impact of an urban canopy and anthropogenic heat fluxes on Sydney's climate. International Journal of Climatology,

37, pp.255-270. https://doi.org/10.1002/joc.5001

Memon, R.A., Leung, D.Y. and Liu, C.H., 2009. An investigation of urban heat island intensity (UHII) as an indicator of urban heating. Atmospheric Research, 94(3), pp.491-500. https://doi.org/10.1016/j.atmosres.2009.07.006

Michel, J.P., 2020. Urbanization and Ageing Health Outcomes. Journal of Nutrition, Health and Aging, 24 :463-465. https://doi.org/10.1007/s12603-020-1360-1

Miles, V. and Esau, I., 2017. Seasonal and spatial characteristics of urban heat islands (UHIs) in northern West Siberian cities. Remote sensing, 9(10), p.989. https://doi.org/10.3390/rs9100989

Nasrallah, H.A., Brazel, A.J. and Balling Jr, R.C., 1990. Analysis of the Kuwait City urban heat island. International Journal of Climatology, 10(4), pp.401-405. https://doi.org/10.1002/joc.3370100407

Nuruzzaman, M. (2015). Urban heat island: causes, effects and mitigation measures-a review. International Journal of Environmental Monitoring and Analysis, 3(2), 67-73. https://doi.org/10.11648/j.ijema.20150302.15

Oke, T.R., 1982. The energetic basis of the urban heat island. Quarterly Journal of the Royal Meteorological Society, 108(455), pp.1-24. https://doi.org/10.1002/qj.49710845502

Prathamesh K Barane. QGIS plugin - NITK_RS-GIS_1.1: LST Calculation. https://github.com/PrathamGitHub/NITK_RS-GIS_17/blob/master/LST_Calculation.pdf. (accessed on 6 October 2020).

Rasul, A.O., 2016. Remote sensing of surface urban cool and heat island dynamics in Erbil, Iraq, between 1992 and 2013 (Doctoral dissertation, University of Leicester).

Reddy, S.N. and Manikiam, B., 2017. Land surface temperature retrieval from LANDSAT data using emissivity estimation. International Journal of Applied Engineering Research, 12(20), pp.9679-9687.

Rossi, F., Bonamente, E., Nicolini, A., Anderini, E. and Cotana, F., 2016. A carbon footprint and energy consumption assessment methodology for UHI-affected lighting systems in built areas. Energy and Buildings, 114, pp.96-103.https://doi.org/10.1016/j.enbuild.2015.04.054

Santamouris, M., 2015. Regulating the damaged thermostat of the cities-Status, impacts and mitigation challenges. Energy and Buildings, 91, pp.43-56.https://doi.org/10.1016/j.enbuild.2015.01.027

Sattari, F., Hashim, M. and Pour, A.B., 2018. Thermal sharpening of land surface temperature maps based on the impervious surface index with the TsHARP method to ASTER satellite data: A case study from the metropolitan Kuala Lumpur, Malaysia. Measurement, 125, pp.262-278. https://doi.org/10.1016/j.measurement.2018.04.092

Shishegar, N., 2014. The impact of green areas on mitigating urban heat island effect: A review. The International Journal of Environmental Sustainability, 9(1), pp.119-130. https://doi.org/10.18848/2325-1077/CGP/v09i01/55081

Solecki, W.D., Rosenzweig, C., Parshall, L., Pope, G., Clark, M., Cox, J. and Wiencke, M., 2005. Mitigation of the heat island effect in urban New Jersey. Global Environmental Change Part B: Environmental Hazards, 6(1), pp.39-49. https://doi.org/10.1016/j.hazards.2004.12.002

Tan, J., Zheng, Y., Tang, X., Guo, C., Li, L., Song, G., Zhen, X., Yuan, D., Kalkstein, A.J., Li, F. and Chen, H., 2010. The urban heat island and its impact on heat waves and human health in Shanghai. International journal of biometeorology, 54(1), pp.75-84. https://doi.org/10.1007/s00484-009-0256-x

Tran, D.X., Pla, F., Latorre-Carmona, P., Myint, S.W., Caetano, M. and Kieu, H.V., 2017. Characterizing the relationship between land use land cover change and land surface temperature. ISPRS Journal of Photogrammetry and Remote Sensing, 124, pp.119-132. https://doi.org/10.1016/j.isprsjprs.2017.01.001

Turco, M., Rosa-Cánovas, J.J., Bedia, J., Jerez, S., Montávez, J.P., Llasat, M.C. and Provenzale, A., 2018. Exacerbated fires in Mediterranean Europe due to anthropogenic warming projected with non-stationary climate-fire models. Nature communications, 9(1), pp.1-9. https://doi.org/10.1038/s41467-018-06358-z

Uddin, S., Al Ghadban, A.N., Al Dousari, A., Al Murad, M. and Al Shamroukh, D., 2010. A remote sensing classification for land-cover changes and micro-climate in Kuwait. International Journal of Sustainable Development and Planning, 5(4), pp.367-377.https://doi.org/10.2495/SDP-V5-N4-367-377

United Nations. United Nations Urbanization and Development: Emerging Futures; World Cities Reports. Available online: https://unhabitat.org/sites/default/files/2020/11/world_cities_report_2020_abridged_version.pdf (accessed on 8 March 2021).

United Nation. Department of Economic and Social Affairs, Population Division. World Urbanization Prospects: The 2018 Revision, Methodology. Report No. ESA/P/WP.252 (New York, NY, USA, 2018). Available online: https://population.un.org/wup/publications/Files/WUP2018-Report.pdf (accessed on 5 March 2021).

Velavan, T.P. and Meyer, C.G., 2020. The COVID-19 epidemic. Tropical medicine and international health, 25(3), p.278. https://doi.org/10.1111/tmi.13383

Wang, S., Fang, C., Guan, X., Pang, B. and Ma, H., 2014. Urbanization, energy consumption, and carbon dioxide emissions in China: A panel data analysis of China's provinces. Applied Energy, 136, pp.738-749. https://doi.org/10.1016/j.apenergy.2014.09.059

Wang, X., Cheng, H., Xi, J., Yang, G. and Zhao, Y., 2018. Relationship between park composition, vegetation characteristics and cool

island effect. Sustainability, 10(3), p.587. https://doi.org/10.3390/su10030587

Wang, Y., Li, Y., Di Sabatino, S., Martilli, A. and Chan, P.W., 2018. Effects of anthropogenic heat due to air-conditioning systems on an extreme high temperature event in Hong Kong. Environmental Research Letters, 13(3), p.034015. https://doi.org/10.1088/1748-9326/aaa848

Wang, Y. and Zhao, T., 2018. Impacts of urbanization-related factors on CO2 emissions: evidence from China's three regions with varied urbanization levels. Atmospheric Pollution Research, 9(1), pp.15-26. https://doi.org/10.1016/j.apr.2017.06.002

Wang, Z., Xing, W., Huang, Y. and Xie, T., 2016. Studying the Urban Heat Island Using a Local Climate Zone Scheme. Polish Journal of Environmental Studies, 25(6).Zhang, X. and Li, H., 2020. The evolving process of the land urbanization bubble: Evidence from Hangzhou, China. Cities, 102, p.102724. https://doi.org/10.1016/j.cities.2020.102724

Weisberg, S., 2005. Applied linear regression (Vol. 528). United States. John Wiley and Sons. https://doi.org/10.1002/0471704091

Zhang, X. and Li, H., 2020. The evolving process of the land urbanization bubble: Evidence from Hangzhou, China. Cities, 102, p.102724. https://doi.org/10.1016/j.cities.2020.102724